Front. Mater. Sci. 2017, 11(4): 328–343
https://doi.org/10.1007/s11706-017-0401-0

RESEARCH ARTICLE

Folate-conjugated pH-responsive nanocarrier designed for active tumor targeting and controlled release of doxorubicin

Lulu WEI[1], Beibei LU[1], Lin CUI[2], Xueying PENG[1], Jianning WU[1], Deqiang LI[3], Zhiyong LIU (✉)[1], and Xuhong GUO[1,4]

1 School of Chemistry & Chemical Engineering, Shihezi University/Key Laboratory of Green Processing for Chemical Engineering/Key Laboratory of Materials-Oriented Chemical Engineering of Xinjiang Uygur Autonomous Region/Engineering Research Center of Materials-Oriented Chemical Engineering of Xinjiang Bingtuan, Shihezi 832003, China
2 School of Medicine, Shihezi University, Shihezi 832003, China
3 College of Chemistry and Chemical Engineering, Xinjiang Agricultural University, Urumqi 830001, China
4 State Key Laboratory of Chemical Engineering, East China University of Science and Technology, Shanghai 200237, China

ABSTRACT: A novel type of amphiphilic pH-responsive folate-poly(ε-caprolactone)-*block*-poly(2-hydroxyethylmethacrylate)-*co*-poly(2-(dimethylamino)-ethylmethacrylate) (FA-PCL-*b*-P(HEMA-*co*-DMAEMA)) (MFP) block copolymers were designed and synthesized *via* atom transfer radical polymerization (ATRP) and ring opening polymerization (ROP) techniques. The molecular structures of the copolymers were confirmed with ^{1}H NMR, FTIR and GPC measurements. The critical micelle concentration (CMC) of MFP in aqueous solution was extremely low (about 6.54 mg/L). The *in vitro* release behavior of DOX-loaded micelles was significantly accelerated when the pH value of solution decreased from 7.4 to 5.0. *In vitro* antitumor efficiency was evaluated by incubating DOX-loaded micelles with Hela cells. The results demonstrated that this copolymer possessed excellent biocompatibility, and FA-decorated micelles MFP showed higher cellular uptake than those micelles without the FA moiety, indicating their unique targetability. These folate-conjugated biodegradable micelles are highly promising for targeted cancer chemothe-rapy.

KEYWORDS: amphiphilic polymer; pH-sensitive; active targeting; drug delivery system; folic acid

Contents

Received July 16, 2017; accepted September 18, 2017

E-mail: lzyongclin@sina.com

1 Introduction

During the past two decades, polymeric micelles or micelle-like nanoparticles self-assembling from amphiphilic block copolymers have received widespread interest for drug delivery systems (DDSs) [1–4], especially due to their unique characteristics such as core–shell structure [5–6], mesoscopic size range [7–8], and prolonged blood circulation [9–10]. The inner hydrophobic core serves as a container for encapsulation of hydrophobic drugs and the outer hydrophilic shell can provide a stable interface between the hydrophobic core and the aqueous medium, which can help these nanoparticles to escape from the reticuloendothelial system (RES) [11–12] uptake after intravenous administration and counterchecks the aggregation of micelles, protects drugs from inactivating under the biological environment, and decreases side effects of drugs on healthy cells and tissues [2,13]. Externally applied stimuli include temperature changes [14], magnetic fields [15], ultrasound [16], light [17], and electric fields [18]; intrinsic stimuli include variations in pH [19], redox potential [20], or the concentrations of enzymes [21].

As well as prioritized accumulation at tumor sites, nanotechnology-based drug delivery system has shown promising results in cancer therapy owing to their improved pharmacokinetics and pharmacodynamics by the enhanced permeation and retention (EPR) effect [22–24]. In particular, self-assembled polymeric micelles have been prominent as promising vehicles based on their distinctive features, i.e. enhanced solubility, high loading capacity, and circulation lifetime of active therapeutics [25–27]. Furthermore the EPR effect exploits preferential uptake of large molecules due to the porous vasculature of tumor tissue, and subsequent retention as a result of poor lymphatic drainage relative to healthy tissue [28]. However, the EPR effect does have several limitations, including poor cellular internalization and inefficient intracellular drug release [29]. To overcome these limitations, two promising strategies were primed: one was to construct an actively targeted drug delivery system and the other was to endow a system stimuli-responsive for controlled drug release.

Based on the above preconditions, among the investigated amphiphilic block copolymers that self-assembly as suitable carriers for controlled drug delivery, biodegradable copolymers were of special interest. By selecting suitable hydrophilic segments, which were resistible toward blood or tissues as the outer shell, the polymeric micelles cannot be recognized by certain proteins or phagocytic cells and finally achieve long-circulation in the blood or tissues [9–10,30], materials such as poly(vinyl alcohol) [16,31], polyacetals [32–33], poly(*b*-hydroxybutyrate) (PHB) [34–35], polylactide (PLA) [19,36–37], and poly(ε-caprolactone) (PCL) [38] were widely used as the hydrophobic segment of amphiphilic block copolymers because of their biocompatibility and biodegradability. The most utilized hydrophilic component is PCL, which is generally synthesized *via* ring opening polymerization (ROP). This is because the PCL is a U.S. Food and Drug Administration (FDA) approved semi-crystalline, with an ester group and five methylene groups in its repeating unit that might be used as a synthetic biomaterial or a controlled drug release matrix due to its good drug permeability, biocompatibility and nontoxicity [39–40]. The active targeting strategy utilizing various targeting ligands that bind to specific proteins overexpressed on cancer cells has provided an opportunity to selectively deliver drugs to the tumor cells *via* receptor-mediated endocytosis [1,41]. Some targeting moieties such as folate (FA) [42–43], peptide [44–45] and biotin [46–47] are covalently linked to the polymer, which can recognize and bind to specific receptors that are selectively over-

expressed on the surface of cancer cells. For instance, the folate, conjugated with an appropriate design, can be directed to the cancer cells in the body and internalized in the target cells *via* receptor-mediated endocytosis. Due to the low-molecular-weight vitamin (M_w = 441.4 g/mol), binding with high affinity to the folate receptor (FR), a membrane-anchored protein has been widely used to modify nanocarriers to further improve the passive targeting systems and accumulate drugs in cancer cells by FR-mediated endocytosis. In the meantime, there is notable intracellular behavior of the folate-bound materials after ligand-mediated endocytosis, which distinguishes the folate ligand from other types of ligands such as antibodies, hormones and peptides. In contrast to the fact that most ligands are internalized and transported to the lysosomes, folate-conjugates remain in recycling endosomes (pH 5.0–6.0) or escape into the cytoplasm, and such a characteristic plays a crucial role in accelerating intracellular uptake of the materials by the cell, avoiding the possible effects of lysosomal enzyme action.

As described above, time-controlled, pH-sensitive, and sustained (not burst release behavior) releases are the most important parts for a successful micelle DDS and much attention has been paid to achieve this goal. For instance, Huang et al. [48] have synthesized a gold nanoparticle with well successfully size-controllable and high stability based on the pH sensitive PDEAEMA segments. Liu et al. [49] have prepared a series of pH- and temperature-responsive star-shaped amphiphiliccopolymers (β-CD-*g*-(PHEMA-*b*-PNIPAM-b-PDMAEMA)), with β-CD-(xanthate) as the initiator and hydroxyethylmethacrylate (HEMA), NIPAM, and 2-(dimethylamino)ethyl methacrylate (DMAEMA) as the pH-responsive monomers. Zhao et al. [42] have constructed polymeric micelles using folate-modified PEOz as hydrophilic corona to enhance the intracellular delivery of anticancer drugs. In this study, we present a facile strategy to control drug release by the variation of environmental pH values, with active targeting capacity based on PCL-*b*-P(HEMA-*co*-DMAEMA) copolymer, decorated with folate ligands. As shown in Scheme 1, this amphiphilic block copolymer was designed and synthesized *via* ATRP and ROP techniques with methyl 2-bromoisobutyrate as the initiator, HEMA and DMAEMA as the monomers. Doxorubicin (DOX) [39,43], one of the most potent applications in tumor therapy, was used as a model drug encapsulated in the micelles of FA-PCL-*b*-P(HEMA-*co*-DMAEMA) (MFP). Moreover, the relation between such intelligent pH-responsive properties of

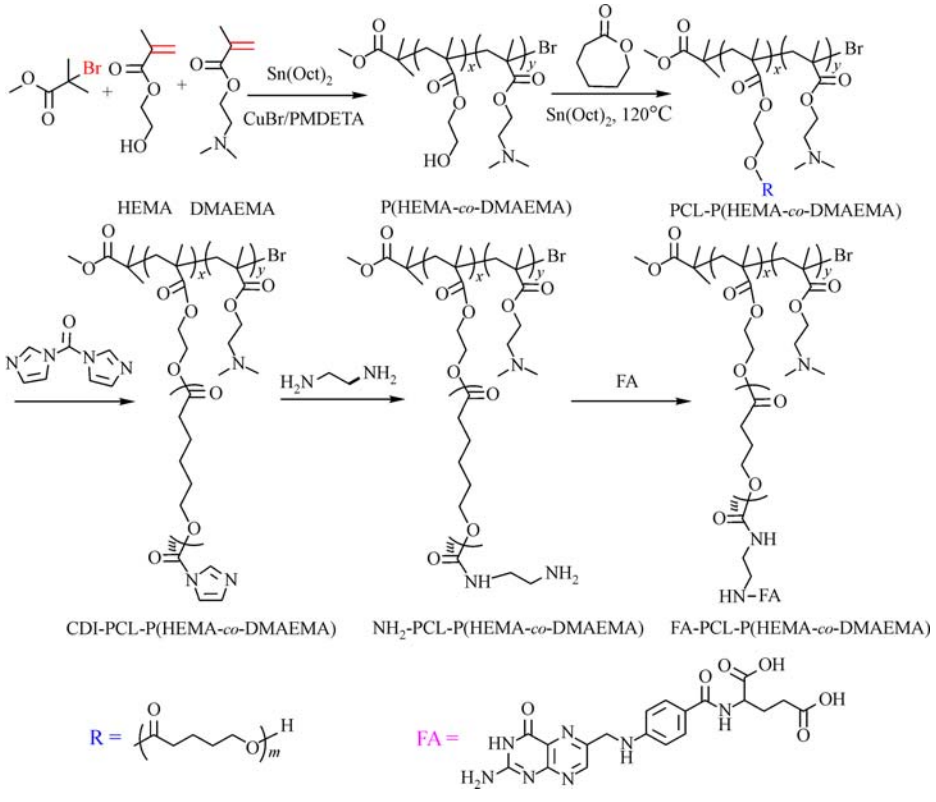

Scheme 1 Synthesis of FA-PCL-P(HEMA-*co*-DMAEMA) copolymer.

micelles and the intracellular uptake as well as cytotoxicity profile and trigged drug release was investigated in detail. Scheme 2 shows the schematic micellization and pH-dependent drug release process of MFP in aqueous solution. The performances of these micelles as drug delivery carriers such as drug loading capacity, *in vitro* drug release behavior, and *in vitro* anticancer activities were investigated in detail.

2 Experimental

2.1 Materials

Methyl 2-bromoisobutyrate (MBriB, 99%, Aldrich), 2-(dimethylamino) ethylmethacrylate (DMAEMA 98%, Aldrich) was filtered over aluminum oxide to remove the inhibitor (MEHQ) before being used. Tin(II) ethylhexanoate ($Sn(Oct)_2$, Sigma), and *N*,*N*′,*N*,*N*″-pentamethyldiethylenetriamine (PMDETA) were purchased from Sigma Aldrich. Copper(I) chloride (99.999%, Alfa Aesar) was used without further purification. ε-CL (Sigma-Aldrich) was distilled under reduced pressure after being treated with CaH_2. Dimethyl sulfoxide (DMSO), *N*,*N*′-dicyclohexylcarbodiimide (DCC), 1,2-ethylenediamine *N*, *N*′-carbonyldiimidazole (CDI), *N*-hydroxysuccinimide (NHS), folic acid (FA), pyrene, dimethylformamide (DMF), dichloromethane (CH_2Cl_2), toluene, trimethylamine (TEA) and tetrahydrofuran (THF) were dried over CaH_2 and distilled before use. Methanol (MeOH), ethanol, diethyl ether, n-hexane, and doxorubicin hydrochloride (DOX·HCl) were purchased from Beijing Huafeng United Technology Co. Ltd. Enhanced Cell Counting Kit-8 (CCK-8) was from Beyotime Biotechnology Co. Ltd., Shanghai. HeLa cells (Institute of Cells, CAS, Shanghai) were used as received. Dulbecco's modified eagle medium (DMEM), fetal bovine serum (FBS), and pancreatic enzymes were obtained from biological industries. 4% Paraformaldehyde, 4',6-diamidino-2-phenylindole (DAPI) and Triton X-100 were purchased from Solarbio.

2.2 Characterization

^1H NMR data were obtained by nuclear magnetic resonance spectroscopy (NMR) using a Bruker DMX-500 NMR spectrometer with $CDCl_3$ as solvent and

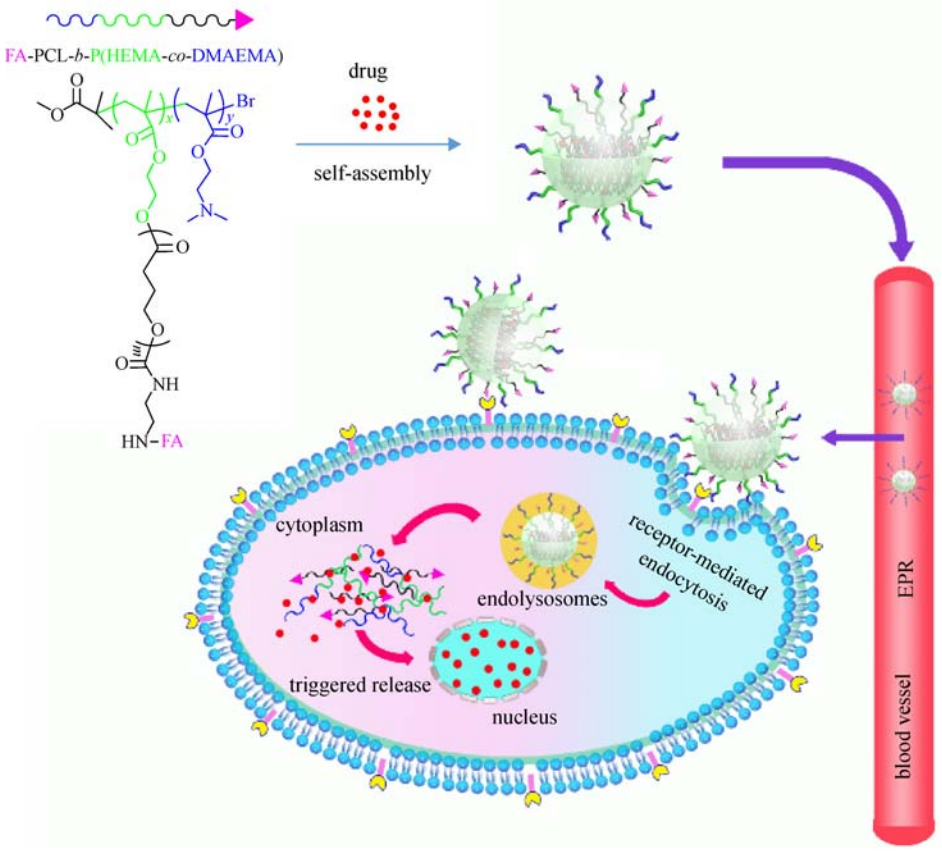

Scheme 2 Scheme of drug entrapping and pH-dependent release from polymeric micelles.

deuterated dimethyl sulfoxide (DMSO-d_6) as solvent and tetramethylsilane (TMS) as an internal standard Fourier transform infrared spectroscopy (FTIR) analysis was measured by Nicolet Avatar 360 using KBr pellets. The molecular weight and molecular weight distribution of copolymers were measured by gel permeation chromatography (GPC) using a Viscotek TDA 302 gel permeation chromatograph and THF was used as eluent. Fluorescence spectra were obtained using a Hitachi F-2500 fluorescence spectrophotometer (F-2500, Hitachi, Japan) and the excitation spectra of polymer/pyrene solutions were scanned from 375 to 395 nm at room temperature, with an emission wavelength of 330 and bandwidth of 5 nm. Dynamic light scattering (DLS) measurements were performed using a BECKMAN COULTER Delasa Nano C particle analyzer at a fixed angle of 165°. Before the light scattering measurements, the sample solutions were filtered three times by using Millipore Teflon (Nylon) filters with a pore size of 0.45 μm. All measurements were repeated three times, and the average result was accepted as the final hydrodynamic diameter (D_h) and zeta potential (mV). Samples for the transmission electron microscopy (TEM) images were taken on an H-600 transmission electron microscope (Hitachi, Japan) operating at 120 kV. Confocal laser scanning microscopy images (Zeiss CLSM510) and fluorescence microscope images (OLYMPUS U-RFL-T, Japan) were obtained at an excitation wavelength of 480 nm.

2.3 Synthesis of P(HEMA-*co*-DMAEMA)

A series of P(HEMA-*co*-DMAEMA) were prepared by ATRP of HEMA and DMAEMA using BIBB as initiator and Cu/PMDETA complex and $Sn(Oct)_2$ as catalyst system and redactor. The reaction procedures were shown in Scheme 1. Briefly, all synthetic procedures were carried out under an argon atmosphere and complied with a standard ATRP instruction [50]. In a typical experiment, 151 mg (1.0 mmol) of CuBr was added into a predried Schlenk flask and sealed with a rubber septum. The flask was degassed and backfilled three times with argon and then left under argon solvent anhydrous (toluene). Subsequently monomer (HEMA) was introduced with syringe and the mixture was conducted with three "freeze-pump-thaw" cycles. A fixed quantity of PMDETA was then injected into the reaction flask after stirring for 15 min, until the solution became homogeneous and the Cu/PMDETA catalyst complex formed. The flask was transferred into a thermostatted oil bath at 60°C, and the polymerization proceeded for 24 h. After being cooled to room temperature, the reaction flask was open to air, and the crude product was diluted with THF and passed through a neutral alumina column to remove the copper catalysts. Finally, it was precipitated thrice into cold hexane. In order to further purify the polymer, the polymer was dissolved in THF, and precipitated three times in cold hexane and dried under vacuum to a constant weight at 40°C. The products with different molar ratios of HEMA to DMAEMA were synthesized by ATRP in the same way, which were named PHD1 (10:20) and PHD2 (10:35).

2.4 ROP of ε-CL in the presence of PCL-P(HEMA-*co*-DMAEMA)

PCL-P(HEMA-*co*-DMAEMA) was synthesized by ROP with ε-CL using $Sn(Oct)_2$ as the catalyst [38–39]. As an example the typical procedure was as follows: P(HEMA-*co*-DMAEMA) (1.15 g, 2.0 mmol), ε-CL (6 g, 52.6 mmol), $Sn(Oct)_2$ (0.04 g, 0.1 mmol), and anhydrous toluene (50 mL) were added into a fresh flamed and nitrogen purged round-bottomed flask. The flask was then placed in a thermostatted oil bath at 120°C for 24 h. After the polymerization, the mixture was cooled to room temperature. The product was dissolved in CH_2Cl_2, and precipitated in methanol three times. Finally, the precipitate was dried under vacuum to a constant weight at 35°C, named P1 (10:20) and P2 (10:35).

2.5 Synthesis of folic acid-attached polymer FA-PCL-P(HEMA-*co*-DMAEMA)

2.5.1 Synthesis of CDI-activated CDI-PCL-P(HEMA-*co*-DMAEMA)

CDI-PCL-P(HEMA-*co*-DMAEMA) was synthesized by a modified procedure as described earlier [12,42]. Briefly, *N*, *N*′-carbonyldiimidazole (CDI) (0.162 g, 1.0 mmol) and PCL-P(HEMA-*co*-DMAEMA) (1.19 g, 2.0 mmol) were respectively dissolved in drydichloromethane. The solution of CDI was added dropwise into the PCL-P(HEMA-*co*-DMAEMA) solution at room temperature for 2 h under nitrogen atmosphere. The mixture was kept stirring for another 4 h. The excess dichloromethane was removed by rotary evaporator. The product was precipitated in ethyl ether for three times to remove unreacted CDI. CDI-PCL-P(HEMA-*co*-DMAEMA) was dried under vacuum to obtain the white powder.

2.5.2 Synthesis of amino-terminated NH_2-PCL-P(HEMA-*co*-DMAEMA)

The anhydrous dichloromethane solution of CDI-PCL-P(HEMA-*co*-DMAEMA) (2.07 g, 3.0 mmol) was added dropwise into 5 mL of 1,2-ethylenediamine at room temperature. The mixture was then reacted overnight. Excess dichloromethane and unreacted 1,2-ethylenediamine were removed by rotary evaporation. The concentrated viscous mixture was poured into an excess amount of cold ethanol to precipitate the product. NH_2-PCL-P(HEMA-*co*-DMAEMA) was dried under vacuum dehydration and collected as yellow powder.

2.5.3 Synthesis of folate-conjugated FA-PCL-P(HEMA-*co*-DMAEMA) copolymer

Folate (1.32 g, 3.0 mmol), NHS (0.35 g, 3.0 mmol), and EDC·HCl (0.57 g, 3.0 mmol) were dissolved in 10 mL DMSO. The mixture was stirred at room temperature under nitrogen atmosphere in the dark overnight. Then, NH_2-PCL-P(HEMA-*co*-DMAEMA) (2.05 g, 3.0 mmol) and several drop of triethylamine were added, and the mixture was reacted for another 24 h. DMSO and unreacted folate were removed by dialysis against deionized water for 3 d. FA-PCL-P(HEMA-*co*-DMAEMA) collected by lyophilization.

2.6 Self-assembly of FA-PCL-P(HEMA-*co*-DMAEMA) in aqueous solution

Samples for UV-vis, DLS and TEM were prepared as follows: FA-PCL-P(HEMA-*co*-DMAEMA) (20 mg) were dissolved in DMSO (2 mL) and subsequently, deionized water (1 mL) was added dropwise from an additional funnel over a period of 30 min. After 4 h quick stirring, 8 mL water was added to quench the micellar assembly, subsequently dialyzed (molecular weight cut-off: 3500 Da) against with distilled water for 72 h. During this dialysis process, the hybridized copolymers self-assembly into micelles with PCL cores and P(HEMA-*co*-DMAEMA) coronas. Polymeric micelles with different concentrations could be obtained by diluting with distilled water and equilibrating at room temperature for 48 h, named MFP1 (10:20) and MFP2 (10:35).

2.7 CMC measurement

The CMC of FA-PCL-P(HEMA-*co*-DMAEMA) was determined by the fluorescence probe technique using pyrene as a fluorescence probe. When polymeric micelles formed, pyrene was preferentially distributed in the hydrophobic micelle core instead of in the hydrophilic outer shell, thus the environment of pyrene turned from polar to nonpolar. The red shift of the third peak indicates that pyrene molecules have been transferred to the less polar domains of micelle core. In a typical experiment, a solution of pyrene (12×10^{-5} mol/L) in acetone was prepared in advance. The polymer was first dissolved into acetone and then confected to a concentration of 0.1 mg/mL with deionized water. After the acetone was evaporated by stirring for 24 h, the polymer solution was diluted to a series of concentrations from 2×10^{-4} to 0.1 mg/mL with deionized water. Pyrene solution (0.1 mL) was added to a vial and the acetone was allowed to evaporate to form a thin film at the bottom of the vial. Then polymer solutions at different concentrations were added to the vials, respectively, and the final concentration of pyrene was 6×10^{-7} mol/L in water. The combined solution of pyrene and copolymer was equilibrated at room temperature in dark for 24 h before measurement. Fluorescence spectra were obtained using a fluorescence spectrophotometer (F-4500, Hitachi) and the excitation spectra of polymer/pyrene solutions were scanned from 375 to 395 nm at room temperature, with an emission wavelength of 330 nm and a bandwidth of 5 nm. The intensity ratio of I_{395} to I_{375} was plotted as a function of logarithm of the polymer concentration. The CMC value was taken from the intersection of the tangent to the curve at the inflection with the horizontal tangent through the points at low concentrations.

2.8 Study on DOX encapsulation and release

100 mg of FA-PCL-P(HEMA-*co*-DMAEMA) and 10 mg of DOX·HCl were dissolved in DMSO (4 mL) separately, and the two solutions were mixed in a vial and stirred for 30 min. A 3-fold excess of TEA was added in order to obtain the DOX base. Then the mixture was added dropwise into water (80 mL) using a syringe pump under high speed stirring. The DOX-containing suspension was then equilibrated under stirring at room temperature for 4 h, followed by thorough dialysis (molecular weight cut-off: 3500 Da) against deionized water for 2 d to remove any unloaded DOX. The obtained DOX-loaded micelles were named D-MFP1 (FA-PCL-P($HEMA_{10}$-*co*-$DMAEMA_{20}$)) and D-MFP2 (FA-PCL-P($HEMA_{10}$-*co*-$DMAEMA_{35}$)). The DOX loading content (DLC) and the DOX loading

efficiency (DLE) were determined using UV-vis spectrophotometry at 480 nm. To determine the drug loading level, a small portion of DOX-loaded micelles was withdrawn and diluted with DMSO to a volume ratio of V(DMSO)/$V(H_2O)$ = 9/1. The amount of DOX encapsulated was quantitatively determined using UV-vis. The calibration curve used for drug loading characterization was established using the intensity of DOX with different concentrations in DMSO/H_2O (9/1, v/v) solutions. The DLC was defined as the weight ratio of entrapped DOX to that of the DOX-loaded micelles. The DLE of DOX was obtained as the weight ratio between the DOX incorporated in the assembled micelles and that used in fabrication:

$$\mathrm{DLC/wt.\%} = \frac{w_{\mathrm{ld}}}{w_{\mathrm{p}}} \times 100 \quad (1)$$

$$\mathrm{DLE/wt.\%} = \frac{w_{\mathrm{ld}}}{w_{\mathrm{df}}} \times 100 \quad (2)$$

where w_{ld} is the weight of loaded drug, w_p is the weight of polymer, and w_{df} is the weight of drug in feed. The *in vitro* DOX release profiles from the polymer assembled micelles were evaluated using buffers solution with pH values 5.0 and 7.4, and then placed in a dialysis bag (molecular weight cut-off: 3500 Da). The whole bag was placed into 35 mL PBS or acetate buffer and shaken (200 r/min) at 37°C.

At specified time intervals 4 mL (V_e) of samples were taken and an equal volume of fresh buffer was added to maintain the total volume. The concentration of DOX in different samples was analyzed by UV-vis spectrophotometry at 480 nm. The cumulative percent drug release (E_r) was calculated using

$$E_{\mathrm{r}}/\% = \frac{V_{\mathrm{e}}\sum_{1}^{n-1} c_i + V_0 c_n}{m_{\mathrm{DOX}}} \times 100 \quad (3)$$

where m_{DOX} represented the amount of DOX in the micelle, V_0 was the volume of the release medium (V_0 = 70 mL), c_i represented the concentration of DOX in the ith sample and c_n represented the concentration of DOX in the nth sample. The *in vitro* release experiments were carried out in triplicate at each pH and the reported results were the average values with standard deviations.

2.9 Cytocompatibility assay

The cytotoxic effects of polymers, free DOX and DOX loaded FA-PCL-P(HEMA-*co*-DMAEMA) micelles were evaluated against HeLa cells by the standard XTT. To perform the cytotoxicity assay, HeLa cells were seeded at a density of 5000 cells per well on a 96-well plate and cultured for 24 h. The samples were prepared at a series of desired concentrations. Every experimental well was treated with the samples for 24 h and others were added with fresh medium as control. After 24 h incubation, CCK-8 was added into each well to dissolve the formazan by pipetting in and out several times. The absorbance of each well was measured at a test wavelength of 450 nm. The cell viability (η) of samples was calculated as follow:

$$\eta/\% = \frac{A_{\mathrm{test}} - A_{\mathrm{blank}}}{A_{\mathrm{control}} - A_{\mathrm{blank}}} \times 100 \quad (4)$$

where A_{test} and $A_{control}$ represent the intensity determined for cells treated with different samples and for control cells, respectively, and A_{blank} is the absorbance of wells without cells.

2.10 Intracellular release of DOX

Confocal laser scanning microscopy (CLSM) was used to visualize the subcellular localization and intracellular release behavior of DOX-loaded micelles and free DOX for various lengths of time (0.5, 4 and 24 h). First, the HeLa cells were seeded in a glass base dish with a coverslip at a density of 5000 cells and cultured in DMEM supplemented with 10% FBS for 24 h. Then DOX-loaded micelles and free DOX was added, and cells were cultured for 0.5, 4 and 24 h in a humidified 5% CO_2-containing atmosphere. Then, the location of intracellular fluorescence was validated using a CLSM imaging system (Zeiss CLSM510) at the excitation wavelength of 480 nm.

2.11 Statistical analysis

The experimental data were presented with an average values, expressed as the mean ± standard deviation (SD). Statistical significance was determined by Student's t-test (Excel, 2007) and considered to be significant when the p values were less than 0.05 ($p < 0.05$).

3 Results and discussion

3.1 Synthesis and characterization of FA-PCL-P(HEMA-*co*-DMAEMA) polymers

The amphiphilic polymers PCL-*b*-P(HEMA-*co*-DMAEMA) was synthesized via a combination of ATRP and ROP, and then modified by folate segment, resulting in triblock pH-sensitive copolymers FA-PCL-P(HEMA-*co*-

DMAEMA) with specific random pH-sensitive/hydrophilic/hydrophobic structure as illustrated in Scheme 1. First of all, the P(HEMA-*co*-DMAEMA) segment was synthesized by using BIBB as initiator and Cu/PMDETA complex and $Sn(Oct)_2$ as catalyst system and redactor, respectively. The polymerization was carried out in anhydrous toluene at 80°C in bulk with a narrow distribution on the condition that the molar ratio of $n(Sn(Oct)_2)/n(CuBr_2)$ was 10/1. The amount of ligand PMDETA was in accord with $Sn(Oct)_2$. A sufficiently large excess of reducing agent $Sn(Oct)_2$ not only reduces Cu(II) to Cu(I) but also is responsible for scavenging oxygen and radical inhibitors. Then ROP of CL occurred to get PCL-P(HEMA-*co*-DMAEMA) in toluene at 120°C for 24 h by using hydroxyterminated P(HEMA-*co*-DMAEMA) as macroinitiator and $Sn(Oct)_2$ as catalyst. Subsequently folate-conjugated triblockamphiphilic copolymer was obtained with the hydrophilic periphery labeled with cancer cell targeting moieties (FA).

The synthesized copolymers and precursors were determined by ^{1}H NMR, as shown in Fig. 1. With regard to precursor P(HEMA-*co*-DMAEMA) (Fig. 1(A)), the characteristic HEMA peak of block copolymers at 3.85 ppm (c) was due to $-CH_2CH_2OH$ protons on the side chain. The signals at 0.91 ppm (g), 1.85 ppm (e), 4.18 ppm (b) were ascribed to $-CCH_3$, $-CCH_2C-$, $-CH_2OCO-$ of the HEMA units, respectively. We found the characteristic signals of the protons in the PDMAEMA block in Figs. 1(A), 1(B) and 1(C). The protons of $-CH_2N-$ and $-CH_3$ of the PDMAEMA block corresponded to the peaks at 2.60 ppm (d) and 0.91 ppm (g), respectively. Furthermore, the overlapped signals at 4.08 ppm (b), 2.32 ppm (f) and 1.82 ppm (e) belonged to the protons of $-COOCH_2CH_2-$, $-N(CH_3)_2$ and $-COOCH_2CH_2-$ in the PDMAEMA block. The structural characteristics of the obtained PCL-P(HEMA-*co*-DMAEMA) and FA-PCL-P(HEMA-*co*-DMAEMA) have been determined by ^{1}H NMR analysis in Figs. 1(B) and 1(C), whereas the resonance at 4.08 ppm (k: $-COOCH_2CH_2-$), 2.32 ppm (h: $-CH_2CH_2CH_2-$), 1.67 ppm (m: $-CH_2CH_2CH_2-$), and 1.39 ppm (i: $-CH_2CH_2OH$) were the characteristic signals of methylene protons at different positions of PCL group respectively, and the characteristic peaks at 3.85 ppm (c) of the PHEMA block disappeared completely in Fig. 1 (B), which indicated that the $-OH$ of PHEMA had reacted. The appearance of the weak signals at 7.4–8.7 ppm corresponded to the aromatic protons of FA molecule in the copolymer in Fig. 1(C). All of these peaks indicate that the

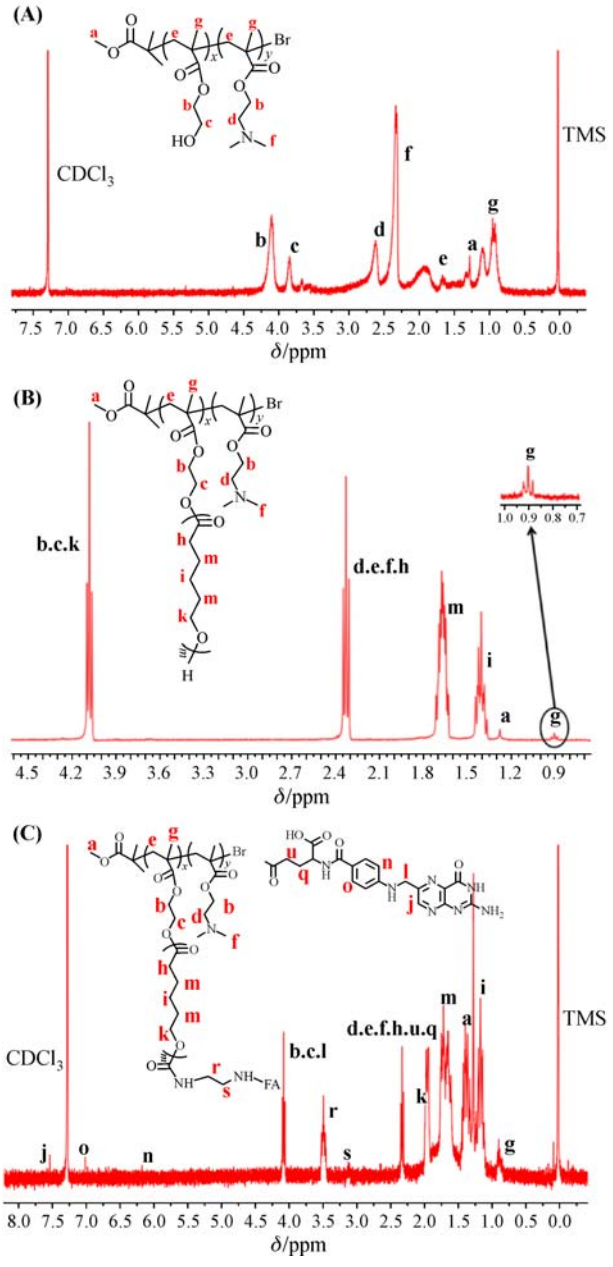

Fig. 1 ^{1}H NMR spectra of **(A)** P(HEMA-*co*-DMAEMA), **(B)** PCL-P(HEMA-*co*-DMAEMA) in $CDCl_3$, and **(C)** FA-PCL-P(HEMA-*co*-DMAEMA) in DMSO-d_6.

FA-PCL-P(HEMA-*co*-DMAEMA) copolymer was successfully synthesized. Subsequently the characterization data of FTIR spectra for P(HEMA-*co*-DMAEMA) and PCL-P(HEMA-*co*-DMAEMA) were summarized in Fig. 2. The infrared analysis for the structure of PCL-P(HEMA-*co*-DMAEMA) showed that there was a wide peak round 3400 cm^{-1} which indicated the stretch vibration of $-OH$ groups. The absorption at 1750 cm^{-1} could be ascribed to the characteristic carbonyl (C = O) stretching vibration of

PCL and PDMAEMA (Curve b in Fig. 2). Two kinds of precursors and block copolymers were synthesized by changing the mole ratio of HEMA to DMAEMA in the first step, and confirmed by GPC and ^{1}H-NMR. The areas of above characteristic peaks were calculated and the results are shown in Table 1. Figure 3 displays the GPC traces of P(HEMA-*co*-DMAEMA) and PCL-P(HEMA-*co*-DMAEMA). The GPC curve of PCL-P(HEMA-*co*-DMAEMA) displays a major distribution that shifts toward the higher-molecular weight side compared with that of P(HEMA-*co*-DMAEMA), indicating that the polymer PCL-P(HEMA-*co*-DMAEMA) has been successfully prepared.

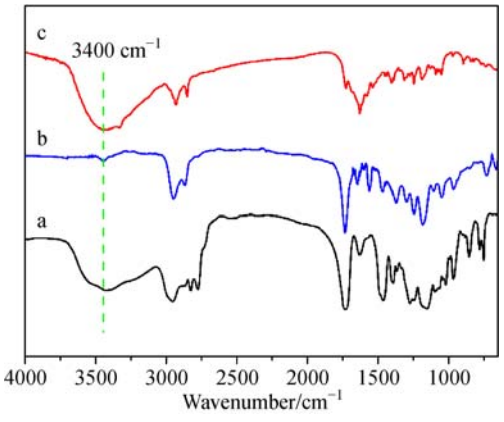

Fig. 2 FTIR spectra of P(HEMA-*co*-DMAEMA) (a), PCL-P(HEMA-*co*-DMAEMA) (b), and FA-PCL-P(HEMA-*co*-DMAEMA) (c).

3.2 Self-assembly and micellar properties of FA-PCL-P(HEMA-*co*-DMAEMA) copolymers

3.2.1 CMC value of FA-PCL-P(HEMA-*co*-DMAEMA)

In order to confirm the formation of micelles self-assembling from FA-PCL-P(HEMA-*co*-DMAEMA), CMC values of FA-PCL-P(HEMA-*co*-DMAEMA) were measured by fluorescence spectroscopy based on selective partition of fluorescence probe in hydrophobic phase against aqueous phase. It has been reported that fluorescence spectra of pyrene solutions contain a vibrational band exhibiting high sensitivity to the polarity of the pyrene environment. The excitation spectra of pyrene at different copolymer concentrations in PBS were acquired and the intensities of absorptions at 395 (I_3) and 375 (I_1) nm were plotted as I_3/I_1 ratio versus FA-PCL-P(HEMA-*co*-DMAEMA) polymer concentration in solution (Fig. 4). As shown in Fig. 4(a), the red shift from 375 to 395 nm is observed when the concentration of FA-PCL-P(HEMA-*co*-DMAEMA) increases from 2×10^{-4} to 0.1 mg/mL. This red shift suggests that pyrene molecules are transferred from the water into the hydrophobic core as well as the formation of micelles. Due to the extremely low CMC values, the micelles formed from FA-PCL-P(HEMA-*co*-DMAEMA) would provide good stability in solution, even after extreme dilution by the larger volume of systemic circulation in the body.

3.2.2 Formation and characterization of the blank and DOX-loaded FA-PCL-P(HEMA-*co*-DMAEMA) (D-MFP1 and D-MFP2) block copolymer micelles

As shown in Scheme 2, as an amphiphilic block copolymer, FA-PCL-P(HEMA-*co*-DMAEMA) could self-assemble into micelles in a selective solvent when the concentration was above the critical micelle concentration (CMC). The particle size, polydispersity index (PDI) and morphology of micelles may be different due to selecting different solvents and operating techniques. In particular, such small size ($<$ 200 nm) property of polymeric micelles was very effective to reduce the level of the nonspecific uptake by the RES and could provide passive tumor targeting ability via the enhanced permeability and retention effect. The physico–chemical properties of the blank and DOX-loaded micelles were characterized using DLS analysis. The hydrodynamic diameter (D_h), PDI and the zeta potentials of the blank and DOX-loaded micelles were summarized in Table 2.

Table 1 GPC and ^{1}H NMR results of copolymer products

Sample	$M_{n,Th}$ [a)]	$M_{n,GPC}$ [b)]	M_w/M_n [b)]	c(HEMA)/c(PDMAEMA)[c)]
Precursor-1	4627	4640	1.47	10/20
Precursor-2	15860	15670	1.50	10/20
Precursor-1'	6985	6870	1.16	10/35
Precursor-2'	18399	25740	1.20	10/35

a) Calculated by monomer feed ratio.
b) Polymerization conditions $[monomer]_0/[2\text{-Bromoisobutyrate}]_0/[CuBr]_0/[PMDETA]_0 = 100/1/1/2$, measured by GPC calibrated with PS standards. THF was used as the eluent.
c) Mole content ratio determined by the integration ratio of ^{1}H NMR spectra. Precursor-1 and 1' were respectively P(HEMA$_{10}$-*co*-DMAEMA$_{20}$)-Br and P(HEMA$_{10}$-*co*-DEAEMA$_{35}$)-Br. Precursor-2 and 2' were respectively PCL-*b*-P(HEMA$_{10}$-*co*-DEAEMA$_{20}$) and PCL-*b*-P(HEMA$_{10}$-*co*-DEAEMA$_{35}$).

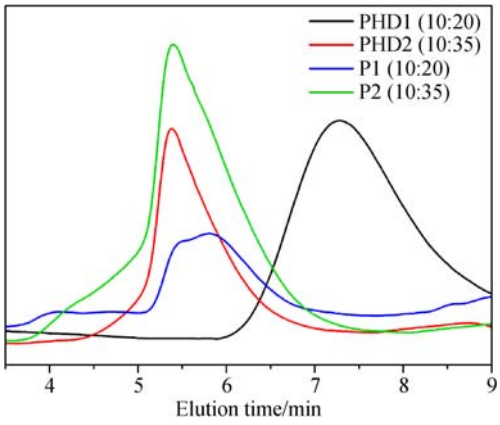

Fig. 3 Evolution of GPC chromatograms of P(HEMA-*co*-DMAEMA) (PHD1 and PHD2) and PCL-P(HEMA-*co*-DMAEMA) (P1 and P2) block copolymers with different molecular weights.

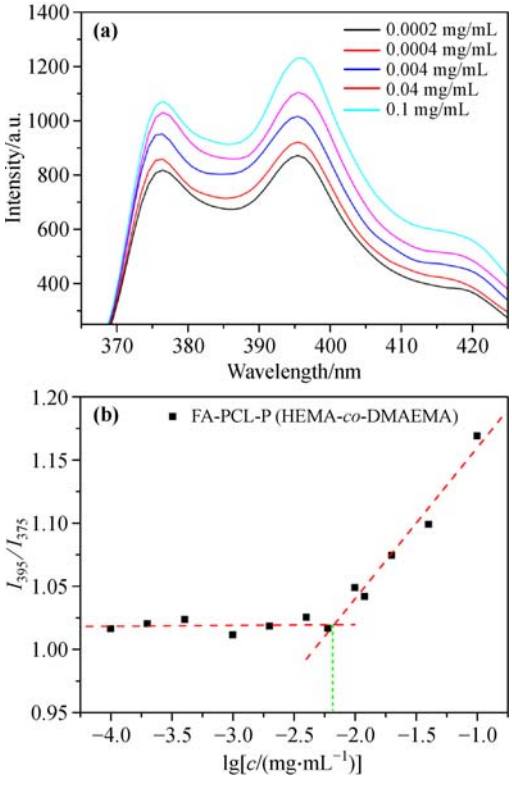

Fig. 4 **(a)** Excitation spectra. **(b)** I_{395}/I_{375} ratio of pyrene in phosphate buffer solution of FA-PCL-P(HEMA-*co*-DMAEMA) at various concentrations.

As shown in Fig. 5, the size distribution histogram of the blank and DOX-loaded micelles in aqueous solution displays a monomodal distribution with an average hydrodynamic diameter.

To further evaluate the properties of micelles, the size and morphology of FA-PCL-P(HEMA-*co*-DMAEMA) micelles were also determined by TEM. As shown in Fig. 6, these block copolymers can aggregate into roughly spherical micelles in PBS, and the average diameter of them was undersize to the result of the DLS measurement. This difference in micelles size measured by TEM and DLS should be attributed to that the latter was the hydrodynamic diameter of micelles in water, whereas the former reveals the morphology size of the micelles in the solid state. When DOX was loaded in the core of polymeric micelles and the drug adsorbed on the surface, it could also be found that the zeta potentials of the drug-loaded micelles were lower than those of the blank micelles for both of the polymers, resulting from the decreased charge density because of the larger particle sizes (Table 2 and Fig. 5). The result revealed that the FA-PCL-P(HEMA-*co*-DMAEMA) micelles could offer the protection of drugs from untimely structure disintegration and premature drug release until arriving at the aim disease sites.

3.3 *In vitro* release of DOX from micelles

The cumulative *in vitro* release of DOX from FA-PCL-P (HEMA-*co*-DMAEMA) was evaluated using PBS buffer solutions (pH = 7.4 and 5.0) at 37°C by using a fluorescence spectrometer, and the results were shown in Fig. 7. The release profiles of DOX showed an obvious initial burst release followed by a sustained release, which was universal for drug carriers. It was also observed that the payload release rates of DOX from the micelles were obviously changed by the pH value as well as time, which was one of the most favorable properties for polymeric nanomicelles. Enhanced release of DOX from the nanomicelles could be clearly observed at pH 5.0 compared to that at pH 7.4. With regard to pH of 7.4 at 37°C, the micelles stayed compact and the loaded DOX was released slowly. After 5 h, less than 20% of DOX (13%

Table 2 Characterization of the blank and DOX-loaded FA-PCL-P(HEMA-*co*-DMAEMA) micelles

Micelle		Properties				
		D_h/nm	PDI	Zeta potential/mV	DLC/wt.%	DLE/wt.%
Blank	MFP1	107±1.4	0.450±0.028	0.52±0.21		
	MFP2	94±2.1	0.512±0.017	0.80±0.32		
DOX-loaded	MFP1	173±2.5	0.553±0.033	−19.07±0.014	6.65	66.5
	MFP2	164±2.8	0.803±0.006	−13.58±0.231	6.88	68.8

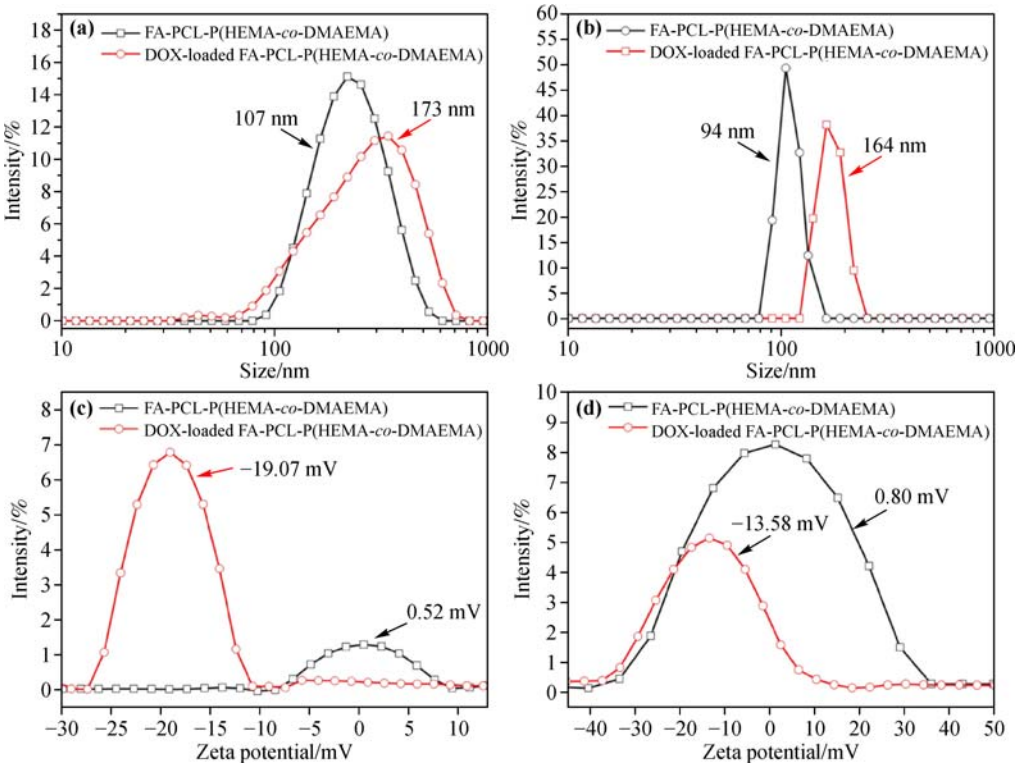

Fig. 5 Particle size distribution curves corresponding to the samples in **(a)** MFP1 and D-MFP1, and **(b)** MFP2 and D-MFP2. Zeta potentials of DOX-loaded polymeric micelles in **(c)** MFP1 and D-MFP1, and **(d)** MFP2 and D-MFP2.

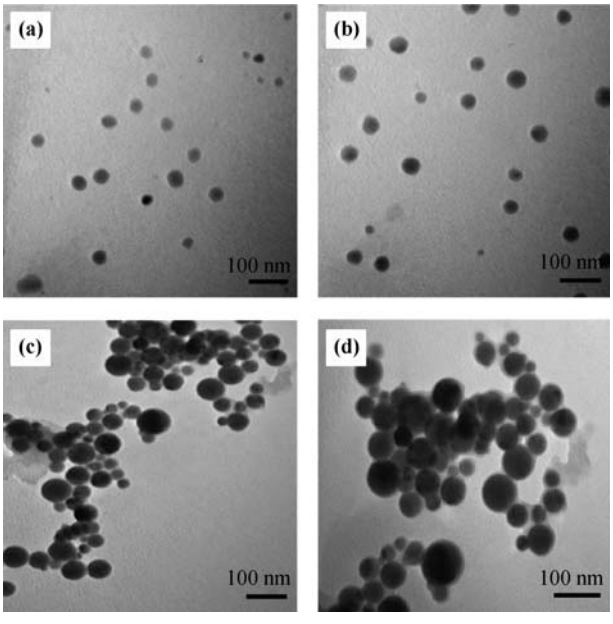

Fig. 6 TEM images: block polymeric micelles **(a)** MFP1 and **(b)** MFP2; DOX-loaded micelles **(c)** D-MFP1 and **(d)** D-MFP2.

and 12% for D-MFP1 and D-MFP2, respectively) were released. Even after 24 h, the data were only about 37% and 29% for D-MFP1 and D-MFP2, respectively. In contrast, when the pH was 5.0 at 37°C, the drug release was accelerated. The cumulative releases after 24 h were 88% and 79% for D-MFP1 and D-MFP2 micelles, respectively.

The payload release accelerated mainly owing to the protonation of tertiary amino groups in DMAEMA of the micelles caused by the decrease of pH values from 7.4 to 5.0. The release profiles showed that the release rate of DOX could be effectively controlled by altering the pH values, the MFP micelles could inhibit the premature burst drug release under the blood circulation conditions which was neutral surroundings and also the DOX release was triggered in acidic surroundings. Furthermore, the accelerated micelle rates might be related to the swollen hydrophobic core which could lead to the drug molecules close to the surface to diffuse into the medium. Meanwhile, the DOX molecules were not only encapsulated inside the micellar core, but also absorbed by the PDMAEMA shell due to the electric action, while only that loaded by hydrophobic effect could be released comparatively fast, so it may spend extended period to achieve complete release. Therefore, these results revealed that the copolymer micelles could have potential applications for the selective release of drugs under intracellular environments.

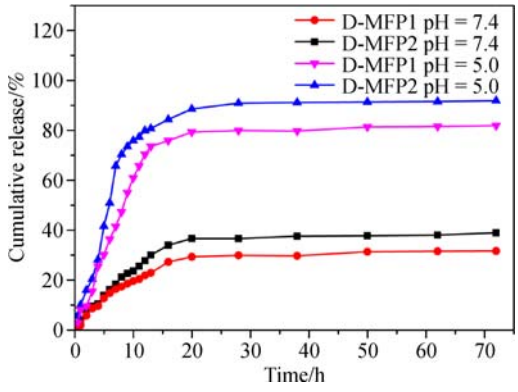

Fig. 7 *In vitro* release of DOX from various DOX-loaded micelles (D-MFP1 and D-MFP2) at 37°C under 7.4 and 5.0 pH conditions.

3.4 Cytotoxicity tests

Cytotoxic effects of the polymers, free DOX or DOX-loaded micelles in HeLa cells were evaluated by CCK-8 assay to demonstrate the superiority of pH-triggered DOX release in our system, as shown in Fig. 8. The cell viability of blank micelles was measured after 48 h incubation. Without loading DOX, all the nanoparticles exhibited a negligible cytotoxicity against HeLa cells at the concentration up to 200 μg/mL. This indicated that all FA-PCL-P(HEMA-*co*-DMAEMA) polymeric micelles were nontoxic and biocompatible and could be used as a delivery system for anticancer agents.

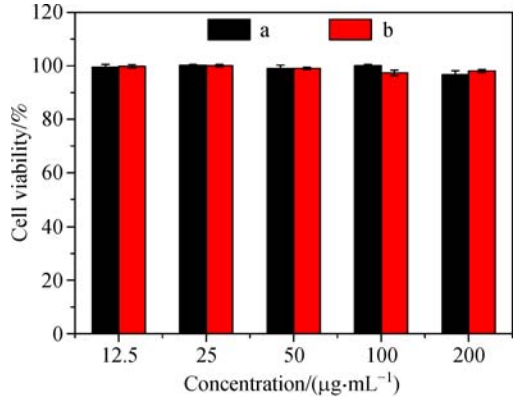

Fig. 8 *In vitro* cell viability of MFP1 (a) and MFP2 (b) micelles. Concentration-dependent cell viability of HeLa cells treated with MFP1 (a) and MFP2 (b) after incubation of 48 h.

Upon drug loading, a drug concentration-dependent cell inhibition was observed as indicated in Fig. 9. HeLa cells were exposed to different doses of DOX and DOX-loaded micelles for 48 h. The cytotoxicity of DOX increased with increasing dose, wherein DOX-loaded micelles exhibited obvious inhibition efficiency at tested DOX equiv. concentration. These results implied that the DOX-loaded micelles system could achieve a low dosage but efficient cancer cell inhibition in chemotherapy, mainly due to the positive surface potential for cell internalization and subsequently the sustained DOX release in the cytoplasm. Nevertheless, the IC_{50} values of free DOX and micelles-encapsulated DOX (the dose having 50% cell inhibition) were 0.619, 1.106, 1.191 μg/mL for 48 h, respectively, suggesting that DOX-loaded micelles possessed less cytotoxic activity than that of free DOX under the same dose. This was likely due to the controlled and incomplete release of DOX from micelles over this time frame. Taken together, these results revealed that DOX released from the micelles could achieve site-specific cell uptake and drug release at weakly acidic tumor microenvironments, which would lead to enhanced tumor inhibition and reduce drug side effects in chemotherapy.

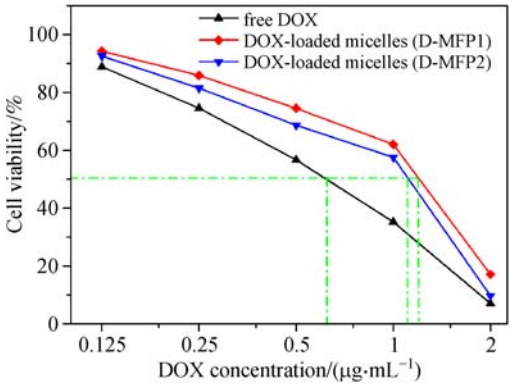

Fig. 9 Cell viability of HeLa cells incubated with free DOX and DOX-loaded micelles (D-MFP1 and D-MFP2) for 48 h at different concentrations.

3.5 *In vitro* cellular uptake studies

The CLSM technique was utilized to evaluate cellular uptake and intracellular drug release behaviors of free DOX and DOX-loaded micelles for HeLa cells, which could synchronously record the dynamic uptake process and the variation of fluorescence intensity using free DOX and DOX-loaded PCL-P(HEMA-*co*-DMAEMA) micelles without FA as a control. Since DOX was fluorescent, its emission was directly used to visualize cellular uptake without additional fluorescence probes. After incubation for 0.5 h, the cell nuclei were stained with DAPI (blue), and the nuclei and cytoplasm of pretreated cells were observed by CLSM. By comparison with the control in Figs. 10(a)

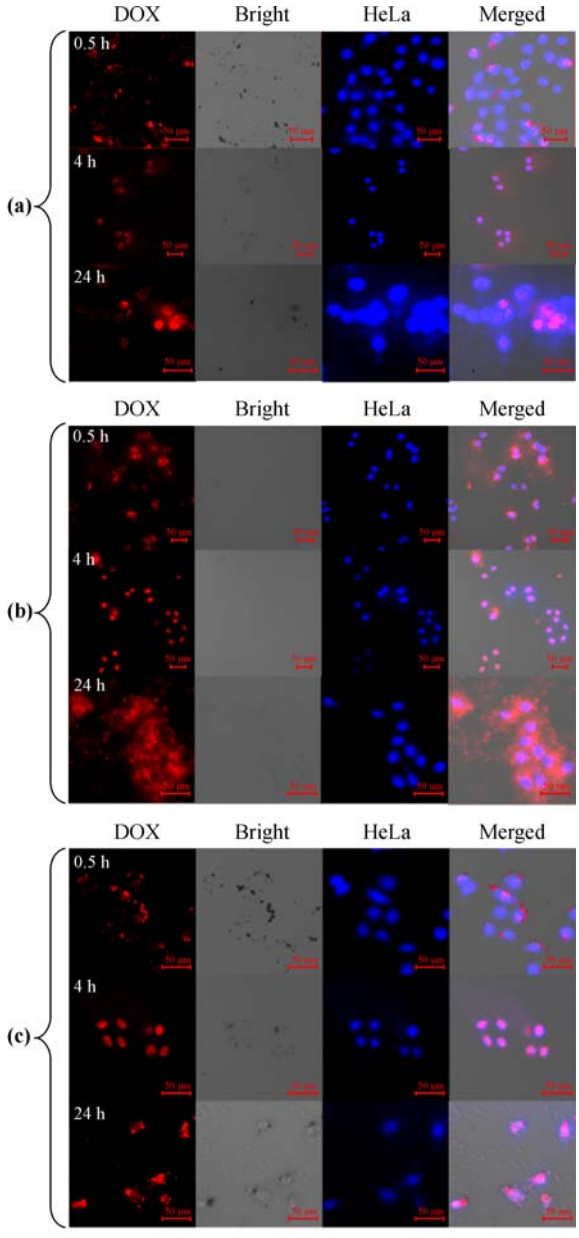

Fig. 10 Confocal laser scanning microscopy images of HeLa cells incubated with **(a)** free DOX and **(b)** DOX-loaded D-P2 for different times, and **(c)** DOX-loaded D-MFP2 for different times. The DOX dosage was 10 mg/mL. For each panel, images from left to right show cell nuclei stained by DOX fluorescence in cells (red), bright field of cells, HeLa (blue), and overlays of the blue and red images. The scale bars are 50 μm in all images.

and 10(b), the observation revealed that free DOX was slightly accumulated in the cell cytoplasm of HeLa cells. Obviously, as shown in Fig. 10(c), DOX-loaded FA-PCL-P(HEMA-*co*-DMAEMA) micelles start internalizing into HeLa cells after 4 h of incubation and the red fluorescence intensity of DOX became gradually stronger with the increase of incubation time, indicating the fast internalization of the DOX-loaded micelles and the efficient release of DOX inside cells. After 24 h incubation, a significant portion of DOX-loaded FA-PCL-P(HEMA-*co*-DMAEMA) micelles was internalized by HeLa cells. In comparison, minimal DOX fluorescence was observed in HeLa cells after being cultured with free DOX for 24 h, as shown in Figs. 10(a) and 10(b). These results confirm that DOX-loaded micelles are likely more efficiently retained inside HeLa cells and have enhanced cytotoxicity as compared to free DOX and DOX-loaded micelles without FA. Similar results have also been reported previously. However, these results came from different internalized mechanisms. Free DOX molecules and DOX-loaded micelles without FA entered tumor cells through the diffusion process depending on the concentration gradient across the cell membrane of tumor cells and further diffused into the nuclei, while the nanocarriers were internalized by FR-mediated endocytosis. Once the micelles are internalized, they may not be pumped out of the cells for a relatively long period. Free DOX can enter into cells fast at first, but it is easy for them to escape from the cells later. We can observe the overlapped color in the merged image, suggesting that the DOX released from DOX-loaded FA-PCL-P(HEMA-*co*-DMAEMA) micelles was distributed in nuclei. In contrast to FA-conjugated micelles, the free DOX and DOX-loaded micelles without FA showed less cellular uptake without the effect of FA ligands. What's more, the red fluorescence located in nucleus must be the drug released from micelles.

4 Conclusions

In summary, a new type of folate-decorated pH-responsive micelles based on the FA-PCL-P(HEMA-*co*-DMAEMA) were developed for the tumor-targeted delivery and pH-induced controlled release of hydrophobic anticancer drugs. The FA-PCL-P(HEMA-*co*-DMAEMA) micelles exhibit without toxic effects on the cultured cells. These multifunctional biocompatible DOX-loaded micelles with well-defined structure and size had excellent colloidal stability with only little drug leakage under physiological conditions and rapidly dissociated with triggered drug release at intracellular acidic and reductive conditions. Furthermore, the introduction of folate into mixed micelles enhanced the cell killing effect *via* that they exhibited enhanced internalization in FA-receptors overexpressed tumor cells *via* the receptor-mediated endocytosis to induce the death of cancer cells compared to the nondecorated free DOX counterparts. Therefore, it can be credible that the

folate-modified pH-sensitive copolymers hold great promise for efficient intracellular delivery and the release of potent hydrophobic anticancer drugs, affording enhanced cancer chemotherapy.

Acknowledgements This work was supported financially by the National Natural Science Foundation of China (Grant Nos. 21367022, 51662036 and 21664013) and the Bingtuan Innovation Team in Key Areas (2015BD003).

References

[1] Chen G, Roy I, Yang C, et al. Nanochemistry and nanomedicine for nanoparticle-based diagnostics and therapy. Chemical Reviews, 2016, 116(5): 2826–2885

[2] Nicolas J, Mura S, Brambilla D, et al. Design, functionalization strategies and biomedical applications of targeted biodegradable/biocompatible polymer-based nanocarriers for drug delivery. Chemical Society Reviews, 2013, 42(3): 1147–1235

[3] Hunter A C, Moghimi S M. Smart polymers in drug delivery: a biological perspective. Polymer Chemistry, 2017, 8(1): 41–51

[4] Qin S Y, Zhang A Q, Cheng S X, et al. Drug self-delivery systems for cancer therapy. Biomaterials, 2017, 112: 234–247

[5] Choi W I, Yoon K C, Im S K, et al. Remarkably enhanced stability and function of core/shell nanoparticles composed of a lecithin core and a pluronic shell layer by photo-crosslinking the shell layer: *in vitro* and *in vivo* study. Acta Biomaterialia, 2010, 6(7): 2666–2673

[6] Cai G, Zhang H, Liu P, et al. Triggered disassembly of hierarchically assembled onion-like micelles into the pristine core–shell micelles via a small change in pH. Acta Biomaterialia, 2011, 7(10): 3729–3737

[7] Song W T, Tang Z H, Zhang D W, et al. A cooperative polymeric platform for tumor-targeted drug delivery. Chemical Science, 2016, 7(1): 728–736

[8] Li H M, Fu Y, Zhang T, et al. Rational design of polymeric hybrid micelles with highly tunable properties to co-deliver microRNA-34a and vismodegib for melanoma therapy. Advanced Functional Materials, 2015, 25(48): 7457–7469

[9] Taghdisi S M, Danesh N M, Ramezani M, et al. Double targeting and aptamer-assisted controlled release delivery of epirubicin to cancer cells by aptamers-based dendrimer *in vitro* and *in vivo*. European Journal of Pharmaceutics and Biopharmaceutics, 2016, 102: 152–158

[10] Zhang C Y, Chen Q, Wu W S, et al. Synthesis and evaluation of cholesterol-grafted PEGylated peptides with pH-triggered property as novel drug carriers for cancer chemotherapy. Colloids and Surfaces B: Biointerfaces, 2016, 142: 55–64

[11] Suo A, Qian J, Zhang Y, et al. Comb-like amphiphilic polypeptide-based copolymer nanomicelles for co-delivery of doxorubicin and P-gp siRNA into MCF-7 cells. Materials Science and Engineering C, 2016, 62: 564–573

[12] Lv Y, Tao L, Annie Bligh S W, et al. Targeted delivery and controlled release of doxorubicin into cancer cells using a multifunctional graphene oxide. Materials Science and Engineering C, 2016, 59: 652–660

[13] Peetla C, Vijayaraghavalu S, Labhasetwar V. Biophysics of cell membrane lipids in cancer drug resistance: Implications for drug transport and drug delivery with nanoparticles. Advanced Drug Delivery Reviews, 2013, 65(13–14): 1686–1698

[14] Li L, Lu B B, Wu J N, et al. Synthesis and self-assembly behavior of thermo-responsive star-shaped POSS-(PCL-P(MEO_2MA-co-PEGMA))$_{16}$ inorganic/organic hybrid block copolymers with tunable lower critical solution temperature. New Journal of Chemistry, 2016, 40(5): 4761–4768

[15] Wang M, Li J, Li X, et al. Magnetically and pH dual responsive dendrosomes for tumor accumulation enhanced folate-targeted hybrid drug delivery. Journal of Controlled Release, 2016, 232: 161–174

[16] Li G, Yan Q, Xia H, et al. Therapeutic-ultrasound-triggered shape memory of a melamine-enhanced poly(vinyl alcohol) physical hydrogel. ACS Applied Materials & Interfaces, 2015, 7(22): 12067–12073

[17] Choi S K, Thomas T, Li M H, et al. Light-controlled release of caged doxorubicin from folate receptor-targeting PAMAM dendrimer nanoconjugate. Chemical Communications, 2010, 46 (15): 2632–2634

[18] Yan Q, Yuan J, Cai Z, et al. Voltage-responsive vesicles based on orthogonal assembly of two homopolymers. Journal of the American Chemical Society, 2010, 132(27): 9268–9270

[19] Sun C Y, Liu Y, Du J Z, et al. Facile generation of tumor-pH-labile linkage-bridged block copolymers for chemotherapeutic delivery. Angewandte Chemie International Edition, 2016, 55(3): 1010–1014

[20] Li D, Bu Y, Zhang L, et al. Facile construction of pH- and redox-responsive micelles from a biodegradable poly(β-hydroxyl amine) for drug delivery. Biomacromolecules, 2016, 17(1): 291–300

[21] Li Y, Liu G, Wang X, et al. Enzyme-responsive polymeric vesicles for bacterial-strain-selective delivery of antimicrobial agents. Angewandte Chemie International Edition, 2016, 55(5): 1760–1764

[22] Maeda H, Nakamura H, Fang J. The EPR effect for macromolecular drug delivery to solid tumors: Improvement of tumor uptake, lowering of systemic toxicity, and distinct tumor imaging *in vivo*. Advanced Drug Delivery Reviews, 2013, 65(1): 71–79

[23] Bose R J C, Lee S H, Park H. Biofunctionalized nanoparticles: an emerging drug delivery platform for various disease treatments.

Drug Discovery Today, 2016, 21(8): 1303–1312

[24] Shi J, Kantoff P W, Wooster R, et al. Cancer nanomedicine: progress, challenges and opportunities. Nature Reviews Cancer, 2017, 17(1): 20–37

[25] Li H J, Du J Z, Du X J, et al. Stimuli-responsive clustered nanoparticles for improved tumor penetration and therapeutic efficacy. Proceedings of the National Academy of Sciences of the United States of America, 2016, 113(15): 4164–4169

[26] Yin Q, Tang L, Cai K, et al. Pamidronate functionalized nanoconjugates for targeted therapy of focal skeletal malignant osteolysis. Proceedings of the National Academy of Sciences of the United States of America, 2016, 113(32): E4601–E4609

[27] Ma Y, Huang J, Song S, et al. Cancer-targeted nanotheranostics: Recent advances and perspectives. Small, 2016, 12(36): 4936–4954

[28] Das A, Theato P. Activated ester containing polymers: opportunities and challenges for the design of functional macromolecules. Chemical Reviews, 2016, 116(3): 1434–1495

[29] Li H J, Du J Z, Liu J, et al. Smart superstructures with ultrahigh pH-sensitivity for targeting acidic tumor microenvironment: instantaneous size switching and improved tumor penetration. ACS Nano, 2016, 10(7): 6753–6761

[30] Ata S, Basak S, Mal D, et al. Synthesis and self-assembly behavior of POSS tethered amphiphilic polymer based on poly(caprolactone) (PCL) grafted with poly(acrylic acid) (PAA) via ROP, ATRP, and CuAAC reaction. Journal of Polymer Research, 2017, 24(2): 2–13

[31] Fu S X, Yang G Q, Wang J, et al. Acid-degradable poly(ortho ester urethanes) copolymers for potential drug carriers: Preparation, characterization, *in vitro* and *in vivo* evaluation. Polymer, 2017, 114: 1–14

[32] DiLauro A M, Zhang H, Baker M S, et al. Accessibility of responsive end-caps in films composed of stimuli-responsive, depolymerizable poly(phthalaldehydes). Macromolecules, 2013, 46(18): 7257–7265

[33] Seo W, Phillips S T. Patterned plastics that change physical structure in response to applied chemical signals. Journal of the American Chemical Society, 2010, 132(27): 9234–9235

[34] Pan J, Li G, Chen Z, et al. Alternative block polyurethanes based on poly(3-hydroxybutyrate-co-4-hydroxybutyrate) and poly(ethylene glycol). Biomaterials, 2009, 30(16): 2975–2984

[35] Saad G R, Elsawy M A, Elsabee M Z. Preparation, characterization and antimicrobial activity of poly(3-hydroxybutyrate-co-3-hydroxyvalerate)-g-poly(N-vinylpyrrolidone) copolymers. Polymer-Plastics Technology and Engineering, 2012, 51(11): 1113–1121

[36] Li Z, Yuan D, Fan X, et al. Poly(ethylene glycol) conjugated poly (lactide)-based polyelectrolytes: synthesis and formation of stable self-assemblies induced by stereocomplexation. Langmuir, 2015, 31(8): 2321–2333

[37] Xu C F, Zhang H B, Sun C Y, et al. Tumor acidity-sensitive linkage-bridged block copolymer for therapeutic siRNA delivery. Biomaterials, 2016, 88: 48–59

[38] Khodaverdi E, Gharechahi M, Alibolandi M, et al. Self-assembled supramolecular hydrogel based on PCL-PEG-PCL triblock copolymer and-cyclodextrin inclusion complex for sustained delivery of dexamethasone. International Journal of Pharmaceutical Investigation, 2016, 6(2): 78–85

[39] Wang M, Zhou C, Chen J, et al. Multifunctional biocompatible and biodegradable folic acid conjugated poly(ε-caprolactone)-polypeptide copolymer vesicles with excellent antibacterial activities. Bioconjugate Chemistry, 2015, 26(4): 725–734

[40] Sun C Y, Shen S, Xu C F, et al. Tumor acidity-sensitive polymeric vector for active targeted siRNA delivery. Journal of the American Chemical Society, 2015, 137(48): 15217–15224

[41] Wang B B, Galliford C V, Low P S. Guiding principles in the design of ligand-targeted nanomedicines. Nanomedicine, 2014, 9 (2): 313–330

[42] Qiu L Y, Yan L, Zhang L, et al. Folate-modified poly(2-ethyl-2-oxazoline) as hydrophilic corona in polymeric micelles for enhanced intracellular doxorubicin delivery. International Journal of Pharmaceutics, 2013, 456(2): 315–324

[43] Qian J, Xu M, Suo A, et al. Folate-decorated hydrophilic three-arm star-block terpolymer as a novel nanovehicle for targeted co-delivery of doxorubicin and Bcl-2 siRNA in breast cancer therapy. Acta Biomaterialia, 2015, 15: 102–116

[44] Zhang Y, Zhou J, Yang C, et al. Folic acid-targeted disulfide-based cross-linking micelle for enhanced drug encapsulation stability and site-specific drug delivery against tumors. International Journal of Nanomedicine, 2016, 11: 1119–1130

[45] Yhee J Y, Song S, Lee S J, et al. Cancer-targeted MDR-1 siRNA delivery using self-cross-linked glycol chitosan nanoparticles to overcome drug resistance. Journal of Controlled Release, 2015, 198: 1–9

[46] Eloy J O, Petrilli R, Chesca D L, et al. Anti-HER2 immunoliposomes for co-delivery of paclitaxel and rapamycin for breast cancer therapy. European Journal of Pharmaceutics and Biopharmaceutics, 2017, 115: 159–167

[47] Palanca-Wessels M C, Booth G C, Convertine A J, et al. Antibody targeting facilitates effective intratumoral siRNA nanoparticle delivery to HER2-overexpressing cancer cells. Oncotarget, 2016, 7(8): 9561–9575

[48] Feng C, Gu L, Yang D, et al. Size-controllable gold nanoparticles stabilized by PDEAEMA-based double hydrophilic graft copolymer. Polymer, 2009, 50(16): 3990–3996

[49] Lu B, Li L, Wu J, et al. Synthesis of a dual pH and temperature

responsive star triblock copolymer based on β-cyclodextrins for controlled intracellular doxorubicin delivery release. New Journal of Chemistry, 2016, 40(10): 8397–8407

[50] Matyjaszewski K, Tsarevsky N V. Macromolecular engineering by atom transfer radical polymerization. Journal of the American Chemical Society, 2014, 136(18): 6513–6533